International Forum on Aeroelasticity and Structural Dynamics
IFASD 2022
13-17 June 2022 Madrid, Spain

IMPROVED MODE TRACKING FOR THE *P-L* FLUTTER SOLUTION METHOD BASED ON AEROELASTIC DERIVATIVES

David Quero[1], **Pierre Vuillemin**[2], **Charles Poussot-Vassal**[2]

[1]DLR (German Aerospace Center), Göttingen, Germany

[2]DTIS (Information Processing and Systems), ONERA (French Aerospace Lab)
Université de Toulouse, 31055 Toulouse, France

Keywords: Flutter, Loewner framework, aeroelastic derivatives, mode tracking

Abstract: In this work an improved mode tracking algorithm is developed for the *p-L* flutter solution method. Compared to the original criterion used for sorting the aeroelastic modes, the approach presented herein uses aeroelastic derivatives in order to predict the flutter solution at the next parameter value. The present method allows for a more robust and efficient sorting of the aeroelastic modes for configurations where the number of real and complex poles resulting from the representation of the aerodynamic term is high, ensuring a proper tracking of the modes corresponding to the structural degrees of freedom. The flutter *p-L* method together with the proposed mode tracking algorithm is applied to a 2 degrees-of-freedom airfoil configuration with high-fidelity unsteady aerodynamics and to the common research aeroelastic model representing a transport aircraft configuration. For the latter, a modified doublet-lattice method valid throughout the complex plane is used for the reference solution, allowing for the first time to validate the *p-L* flutter solution method for general configurations. The results show that the *p-L* method is able to truly represent the aeroelastic damping when compared to the classical *p-k* and *g* methods.

1 INTRODUCTION

For the design of modern aircraft a number of computations are done in order to ensure that the flying vehicle does not encounter flutter instabilities. This is required at a combination of various parameter values, including the flight condition and different mass configurations. Different methods for the solution of the flutter equation have been proposed, among them the extensively used *p-k* [1] and *g* methods [2]. The generalized aeroelastic analysis method (GAAM) of Edwards and Wieseman [3], unlike the *p-k* and *g* methods, is able to represent the true aeroelastic damping at the cost of computing the aerodynamic forces throughout the complex plane. Recently, the GAAM method has been made available when considering subsonic compressible unsteady aerodynamics modeled by the doublet-lattice method (DLM) [4] and is used in this work for the validation of the *p-L* flutter solution method for general non-planar configurations. The *p-L* flutter solution method presented by Quero et al. [5] is also able to represent the true aeroelastic damping but restricting the computation of the generalized aerodynamic forces (GAF) solely to the imaginary axis, providing an efficient solution compared to the GAAM. The original criterion for the tracking of aeroelastic modes proposed in [5] may not be robust for configurations including a considerable number of structural modes and complex unsteady aerodynamics requiring a high number of (real and complex) poles for its appropriate representation in the complex Laplace domain.

Note that typically the chosen aerodynamic poles for classical rational function approximation techniques (RFA) [6–10] are imposed to have zero imaginary part. This can be directly related to a limitation to physically represent the unsteady aerodynamic forces in the transonic regime, as with increasing Mach number and steady angle of attack conditions buffet may eventually appear. The buffet onset can be predicted with the (linearized) unsteady Reynolds-averaged Navier-Stokes equations (URANS) [11, 12] or with the equivalent counterpart in the frequency domain. The cross of a complex pair of aerodynamic eigenvalues determines the buffet onset, which is known to have a fundamental frequency dictated by the imaginary part of this eigenvalue pair. The existence of this complex aerodynamic pole approaching the imaginary axis manifests itself as a clear peak in the real axis with growing magnitude when increasing, for instance, the angle of attack for fixed Mach and Reynolds numbers [13]. Thus, when approaching the buffet onset the aerodynamic poles must necessarily be complex in order to represent this physical behavior. This is indeed considered by the *p-L* method, where the poles corresponding to the frequency-domain representation of the aerodynamic term are automatically assigned. The existence of these aerodynamic complex poles together with a significant number of structural modes for complex configurations may render the task of sorting the aeroelastic modes more complex, which is the reason for proposing a new mode tracking algorithm.

Several works aimed at improving the mode tracking algorithm for the flutter problem, although none of them are readily applicable to the *p-L* flutter solution method due to its specific formulation as a linear generalized eigenvalue problem. When solving the flutter equation for either the *p-k* and *g* methods or the GAAM by the method of determinant iteration [1] or alternatively by successive approximations [14] only the information related to the eigenvalue at the previous parameter value is used within the solution process. Chen [2] additionally considered the derivatives of the aeroelastic eigenvalues for a predictor-corrector scheme specifically tailored to a reduced frequency sweep for the *g* flutter solution method. Colo et al. [15] proposed the method of invariant pairs in order to prevent missing some roots. An alternative to these limitations is to include additional information from the aeroelastic eigensolution into the flutter solution method itself, as first proposed by Van Zyl [16], who combined the method of successive approximations, eigenvalue solvers handling repeated eigenvalues, and a dedicated scalar product including the aeroelastic (right) eigenvectors for the proper sorting of the obtained aeroelastic modes.

Following Van Zyl's proposal [16], several criteria making use of the information provided by the left and right aeroelastic eigenvectors have been presented. Eldred et al. [17] applied two approaches to the *p-k* flutter solution method, namely, the complex higher-order eigenpair perturbation algorithm and the complex cross-orthogonality check method. Recently Hang et al. [18] have presented an additional criterion which employs two orthogonality checking matrices using left and right aeroelastic eigenvectors, but do not consider the aeroelastic derivatives.

Instead of iteratively applying common eigenvalue solvers in order to find the solution to the flutter equation, nonlinear algebraic solvers may alternatively be used, which may in turn be combined with continuation methods to ensure the proper tracking of the aeroelastic eigensolution. In this case, the information of the aeroelastic eigenvalues and importantly from the eigenvectors are readily considered through the aeroelastic derivatives, used either by the nonlinear solution method itself (when building the Jacobian) or for the predictor-corrector scheme required by the continuation method. Cardani and Mantegazza [19] first used aeroelastic derivatives with respect to the airspeed for the continuation of the flutter solution, inherently assuming the *p-k* approximation for the aerodynamic term. The method consists of a (Huen) predictor -

(Newton) corrector scheme to automatically reduce the speed interval if required. Meyer et al. [20] extended the continuation method by choosing the proper continuation parameter at each step based on information from the tangent method, explicitly addressing the numerical problem caused by the existence of limit points and mode switching. Note that the required aeroelastic derivatives depend on the specific representation chosen for the aerodynamic term throughout the complex Laplace plane. This topic has recently been addressed by Kaiser and Quero [21] and the interested reader is referred to the discussions therein.

Considering the previous ideas, the present work uses the information provided by the aeroelastic derivatives in order to improve the mode tracking algorithm when solving the flutter equation by the *p-L* method. By considering the advantages that previous works report on using the aeroelastic derivatives for a tracking of the aeroelastic eigensolution, in this work the aeroelastic derivatives are obtained by considering the corresponding linear generalized eigenvalue formulation of the *p-L* flutter solution method. Note that in this case the tracking problem corresponds to the proper *sorting* of the available aeroelastic roots, which are all obtained at once [5]. This is different from the case when a nonlinear scheme is applied to the flutter equation (either by iteratively applying common linear eigenvalue solvers or by the use of nonlinear algebraic solvers), where the proper tracking in the context of *continuation* methods may directly affect the solution at the next parameter value.

Regarding the structure of this work, Section 2 briefly describes the *p-L* flutter solution method and provides the aeroelastic derivatives together with the mode tracking criteria. Application cases are considered in Section 3, including the flutter stability boundary computation of a 2 degrees-of-freedom (dof) airfoil with high-fidelity unsteady aerodynamics and of the common research model/flutter reduced order assessment (CRM/FERMAT) transport aircraft configuration. In order to show the validity of the *p-L* flutter solution method, the resulting flutter curves are compared against previous classical flutter solution techniques corresponding to the *p-k* and *g* methods. For the CRM/FERMAT configuration the damping curves obtained by the *p-L* flutter solution method are additionally compared against the GAAM, which required applying a modified doublet-lattice method (DLM) valid throughout the complex Laplace plane [4]. This shows for the first time the ability of the *p-L* flutter solution method of truly representing the aeroelastic damping for general configurations.

2 THE *P-L* FLUTTER SOLUTION METHOD

The *p-L* flutter solution method relies on the solution of the following linear generalized eigenvalue problem [5]:

$$
\begin{aligned}
&\begin{bmatrix} \mathbf{I} & \mathbf{0} & \mathbf{0} \\ \mathbf{0} & \mathbf{I} & \mathbf{0} \\ \mathbf{0} & \mathbf{0} & \mathbf{E}_a\left(M_\infty\right) \end{bmatrix} \frac{d}{dt}\left(\begin{bmatrix} \mathbf{u}_h \\ \frac{d\mathbf{u}_h}{dt} \\ \mathbf{x}_a \end{bmatrix}\right) \\
&= \begin{bmatrix} \mathbf{0} & \mathbf{I} & \mathbf{0} \\ -\mathbf{M}_{hh}^{-1}\mathbf{K}_{hh} & -\mathbf{M}_{hh}^{-1}\mathbf{B}_{hh} & \mathbf{M}_{hh}^{-1} q_{dyn}\left(\frac{U_\infty}{L_{ref}}\right)\mathbf{C}_a\left(M_\infty\right) \\ \mathbf{B}_a\left(M_\infty\right) & \mathbf{0} & \left(\frac{U_\infty}{L_{ref}}\right)\mathbf{A}_a\left(M_\infty\right) \end{bmatrix} \begin{bmatrix} \mathbf{u}_h \\ \frac{d\mathbf{u}_h}{dt} \\ \mathbf{x}_a \end{bmatrix} \\
&= \mathbf{E}_{ae}\left(M_\infty\right)\frac{d}{dt}\mathbf{x}_{ae} = \mathbf{A}_{ae}\left(M_\infty, U_\infty, q_{dyn}\right)\mathbf{x}_{ae},
\end{aligned} \tag{1}
$$

where $\mathbf{u}_h$ contain n_h generalized coordinates, $\mathbf{x}_a$ the set of n_a aerodynamic states and $\mathbf{M}_{hh}$, $\mathbf{B}_{hh}$ and $\mathbf{K}_{hh}$ correspond to the generalized stiffness, damping and mass matrices representing

the dynamic structural model. The reference length used for the reduced frequency definition $k = \omega L_{ref}/U_\infty$ is denoted by L_{ref}. The matrices $\mathbf{E}_a(M_\infty)$, $\mathbf{A}_a(M_\infty)$, $\mathbf{B}_a(M_\infty)$ and $\mathbf{C}_a(M_\infty)$ represent the aerodynamic transfer function matrix which interpolates the generalized aerodynamic forces (GAF) over the imaginary axis and is used throughout the complex plane due to the appropriate extrapolation properties of rational functions [5]. They depend on the Mach number $M_\infty = U_\infty/a_\infty$, with a_∞ the speed of sound. Relying on the unsteady aerodynamic theory under consideration, these aerodynamic matrices may additionally depend on the steady flow state (determined by the angle of attack, sideslip angle and steady aircraft deformation) and on the Reynolds number. For the sake of clarity, only the explicit dependency on the Mach number M_∞ is kept. Finally, the true airspeed U_∞ together with the dynamic pressure $q_{dyn} = \rho_\infty U_\infty^2/2$, where ρ_∞ indicates the freestream density, allow for the variation of parameters leading to the determination of the aeroelastic modes for different flight conditions. They are obtained by solving the linear generalized eigenvalue problem with generalized eigenvalue $\lambda \in \mathbb{C}$ and generalized eigenvector $\boldsymbol{\phi} \in \mathbb{C}^{2n_h+n_a}$ upon application of the Laplace transform to Eq. 1:

$$\left(\lambda \mathbf{E}_{ae}(M_\infty) - \mathbf{A}_{ae}(M_\infty, U_\infty, q_{dyn})\right)\boldsymbol{\phi} = \mathbf{0}, \tag{2}$$

requiring for a proper sorting of the $2n_h + n_a$ roots, assigning n_h of them to those corresponding to the structural dof.

As a side note, the *p-L* flutter solution method may be reformulated as a nonlinear eigenvalue problem by considering the aerodynamic transfer matrix function used for the interpolation of the GAF over the imaginary axis,

$$\mathbf{Q}_{hh}(p, M_\infty) = \mathbf{C}_a(M_\infty)\left(p\mathbf{E}_a(M_\infty) - \mathbf{A}_a(M_\infty)\right)^{-1}\mathbf{B}_a(M_\infty),$$

and inserting it into the original formulation of the flutter equation as function of the complex variable $p = sL_{ref}/U_\infty$:

$$\begin{aligned}
&\Bigg[p^2\left(\frac{U_\infty}{L_{ref}}\right)^2\mathbf{M}_{hh} + p\left(\frac{U_\infty}{L_{ref}}\right)\mathbf{B}_{hh} + \mathbf{K}_{hh} \\
&- q_{dyn}\mathbf{C}_a(M_\infty)\left(p\mathbf{E}_a(M_\infty) - \mathbf{A}_a(M_\infty)\right)^{-1}\mathbf{B}_a(M_\infty)\Bigg]\mathbf{u}_h(p) \\
&= \mathbf{F}_{hh}(p, M_\infty, U_\infty, q_{dyn})\,\mathbf{u}_h(p) = \mathbf{0}.
\end{aligned} \tag{3}$$

This corresponds to a nonlinear eigenvalue problem due to the nonlinear dependence on p, and thus, constitutes the nonlinear variant of the *p-L* flutter solution method. The criteria presented in Section 2.2, which depends on the parameter chosen for the flightpoint definition (airspeed U_∞, density ρ_∞, altitude h or Mach number M_∞), may be readily combined with Eq. 3 resulting in a *continuation* method for the determination of the aeroelastic eigensolution. However, in the rest of this work, the formulation corresponding to a linear generalized eigenvalue problem as in Eq. 2 is chosen, as efficient algorithms for its solution, providing all roots at once, are available [22].

For a known aircraft structure with fixed $\mathbf{M}_{hh}$, $\mathbf{B}_{hh}$ and $\mathbf{K}_{hh}$ matrices and fixed reference length L_{ref} the aeroelastic modes depend on the dynamic pressure $q_{dyn} = \rho_\infty U_\infty^2/2$, the Mach number M_∞ and the airspeed U_∞, see Eq. 2. For more complex unsteady aerodynamic theories they additionally depend on the Reynolds number Re and the aircraft steady-state, defined by the steady angle of attack, sideslip angle and the steady airframe deformation. For the sake of clarity, the dependencies on the Reynolds number and the steady state condition are neglected in the following. The Mach number M_∞ and the airspeed U_∞ are linked by the relation $M_\infty = U_\infty/\sqrt{\gamma R_g T_\infty}$, where T_∞ is the freestream temperature. The heat capacity ratio is $\gamma = 1.4$ and the ideal gas constant $R_g = 287.05287\ \ (Nm/\left(kgK\right))$, both for dry air. Different scenarios can be distinguished depending on how the parametric variation for the determination of the aeroelastic modes, computed by Eq. 2 for the *p-L* method, are considered:

- Case 1. Mach number M_∞ constant, density ρ_∞ constant and increase in the airspeed U_∞. The dynamic pressure and temperature vary quadratically with the airspeed U_∞ according to the relations $q_{dyn} = \rho_\infty U_\infty^2/2$ and $T_\infty = U_\infty^2/\left(\gamma R_g M_\infty^2\right)$.
- Case 2. Mach number M_∞ constant, airspeed U_∞ constant and increase in the density ρ_∞. The dynamic pressure varies linearly with the density as $q_{dyn} = \rho_\infty U_\infty^2/2$ and the temperature remains constant as given by $T_\infty = U_\infty^2/\left(\gamma R_g M_\infty^2\right)$.
- Case 3. Mach number M_∞ constant, decrease in the altitude h and use of the atmospheric relations $\rho_\infty\left(h\right)$ and $T_\infty\left(h\right)$. The corresponding airspeed is determined with $U_\infty = M_\infty\sqrt{\gamma R_g T_\infty\left(h\right)}$, which defines the dynamic pressure as $q_{dyn} = \rho_\infty\left(h\right) M_\infty^2 \gamma R_g T_\infty\left(h\right)/2$.
- Case 4. Altitude h constant, increase in the airspeed U_∞ and use of atmospheric relations $\rho_\infty\left(h\right)$ and $T_\infty\left(h\right)$. The Mach number variation is then given linearly by U_∞ as $M_\infty = U_\infty/\sqrt{\gamma R_g T_\infty\left(h\right)}$ and the dynamic pressure by $q_{dyn} = \rho_\infty\left(h\right) U_\infty^2/2$.

Note that cases 1 and 2 do not consider the standard atmospheric relations and as such they may be thought as corresponding to virtual conditions or achieved at a wind tunnel. Cases 3 and 4 do consider the atmospheric conditions, which may be defined by the international standard atmosphere (ISA) relations specifying the freestream density and temperature, $\rho_\infty\left(h\right)$ and $T_\infty\left(h\right)$, as a function of the altitude h [23]. In this work cases 1 through 3 are considered and the corresponding analytical derivatives provided in Appendix A. Case 4 requires the partial derivative of the matrices $\mathbf{A}_a\left(M_\infty\right)$, $\mathbf{B}_a\left(M_\infty\right)$, $\mathbf{C}_a\left(M_\infty\right)$ and $\mathbf{E}_a\left(M_\infty\right)$ with respect to the Mach number, which in the current setting is not recommended as the aerodynamic states may not be consistent throughout the Mach number. However, the extension of the *p-L* flutter solution method to an explicit parametric dependency on the Mach number within the Loewner framework shall allow to determine these derivatives and is currently under investigation [24]. Note that the aerodynamic state consistency for the generation of aeroelastic models has been addressed in the literature [25–27], but none of these works made use of the Loewner framework as required by the *p-L* flutter solution method.

2.1 Aeroelastic derivatives

In order to improve the tracking of the computed aeroelastic modes at different conditions, the information provided by the derivatives of the eigenvalue and eigenvector under consideration with respect to the parameter of interest β (which can be set to the airspeed U_∞, density ρ_∞, altitude h or Mach number M_∞ according to the cases listed in Section 2) is taken into account. As described in Section 1 this concept has been previously used in the context of numerical continuation while solving the flutter equation as a set of nonlinear algebraic equations [19] and is adapted in the current work to the specific formulation of the *p-L* flutter solution method as a linear generalized eigenvalue problem. Also, the proposed algorithm extends the predictor-

corrector scheme presented by Chen [2] by additionally including the information from the eigenvector derivatives.

Assume that the solution defined by the linear generalized eigenvalue problem of Eq. 2 at a stage j, defined by a particular value of the parameter β, is known and the corresponding aeroelastic modes are properly sorted when compared to the wind-off structural modes. This can be readily achieved by assuming a parametric value with a corresponding small dynamic pressure value, say, $q_{dyn} = 0.1$ (Pa), and comparing the imaginary part of the eigenvalues obtained with Eq. 2 with the wind-off structural frequencies. For the next value of the parameter β at the stage $j+1$ associated with an increase in the dynamic pressure q_{dyn}, a first-order Taylor approximation may be applied provided the change in the aeroelastic eigensolution is *small*:

$$\tilde{\lambda}^{(j+1)} = \lambda^{(j)} + \left(\frac{d\lambda}{d\beta}\right)^{(j)} \Delta\beta, \;\; \tilde{\boldsymbol{\phi}}^{(j+1)} = \boldsymbol{\phi}^{(j)} + \left(\frac{d\boldsymbol{\phi}}{d\beta}\right)^{(j)} \Delta\beta \tag{4}$$

Thus, the each eigensolution at the next parameter value $\beta^{(j+1)} = \beta^{(j)} + \Delta\beta$ may be estimated once the derivative terms $(d\lambda/d\beta)^{(j)}$ and $(d\boldsymbol{\phi}/d\beta)^{(j)}$ are known. In order to obtain them, Eq. 2 is derived with respect to the parameter β (note that for the sake of clarity the explicit dependency of the aerodynamic derivatives on the Mach number M_∞ is not shown):

$$\left(\mathbf{A}_{ae} - \lambda^{(j)}\mathbf{E}_{ae}\right)\left(\frac{d\boldsymbol{\phi}}{d\beta}\right)^{(j)} + \left(\frac{d\mathbf{A}_{ae}}{d\beta} - \left(\frac{d\lambda}{d\beta}\right)^{(j)}\mathbf{E}_{ae} - \lambda^{(j)}\frac{d\mathbf{E}_{ae}}{d\beta}\right)\boldsymbol{\phi}^{(j)} = \mathbf{0}. \tag{5}$$

Noticing that the generalized aeroelastic eigensolution obtained by Eq. 2 does not result in unique eigenvectors (only their direction is determined), an additional constraint is introduced with help of the weighting matrix $\mathbf{W}$,

$$\left(\boldsymbol{\phi}^{(j)}\right)^T \mathbf{W}\boldsymbol{\phi}^{(j)} = W_0. \tag{6}$$

Similarly, Eq. 6 is derived with respect to the parameter β and by choosing a matrix $\mathbf{W}$ which is real and symmetric the resulting three terms on the left-hand side can be collected in two:

$$\begin{aligned}&\left(\frac{d\boldsymbol{\phi}^T}{d\beta}\right)^{(j)} \mathbf{W}\boldsymbol{\phi}^{(j)} + \left(\boldsymbol{\phi}^{(j)}\right)^T \frac{d\mathbf{W}}{d\beta}\boldsymbol{\phi}^{(j)} + \left(\boldsymbol{\phi}^{(j)}\right)^T \mathbf{W}\left(\frac{d\boldsymbol{\phi}}{d\beta}\right)^{(j)} \\ &= \left(\boldsymbol{\phi}^{(j)}\right)^T \frac{d\mathbf{W}}{d\beta}\boldsymbol{\phi}^{(j)} + 2\left(\boldsymbol{\phi}^{(j)}\right)^T \mathbf{W}\left(\frac{d\boldsymbol{\phi}}{d\beta}\right)^{(j)},\end{aligned} \tag{7}$$

which together with Eq. 5 form a linear system of complex equations for the determination of the aeroelastic derivatives $(d\lambda/d\beta)^{(j)}$ and $(d\boldsymbol{\phi}/d\beta)^{(j)}$:

$$\begin{bmatrix} -\mathbf{E}_{ae}\boldsymbol{\phi}^{(j)} & \mathbf{A}_{ae} - \lambda^{(j)}\mathbf{E}_{ae} \\ \mathbf{0} & 2\left(\boldsymbol{\phi}^{(j)}\right)^T \mathbf{W} \end{bmatrix} \begin{bmatrix} \left(\frac{d\lambda}{d\beta}\right)^{(j)} \\ \left(\frac{d\boldsymbol{\phi}}{d\beta}\right)^{(j)} \end{bmatrix} = \begin{bmatrix} -\left(\frac{d\mathbf{A}_{ae}}{d\beta} - \lambda^{(j)}\frac{d\mathbf{E}_{ae}}{d\beta}\right)\boldsymbol{\phi}^{(j)} \\ -\left(\boldsymbol{\phi}^{(j)}\right)^T \frac{d\mathbf{W}}{d\beta}\boldsymbol{\phi}^{(j)} \end{bmatrix}, \tag{8}$$

Note that the use of the additional constraint given by Eq. 6 requires the scaling of the eigenvectors obtained after solving the linear generalized eigenvalue defined by Eq. 2. In this work the matrix $\mathbf{W}$ is chosen to be diagonal, with a value of 1 in the first n_h diagonal entries and the rest of the diagonal (and off-diagonal) entries being zero,

$$\mathbf{W} = \begin{bmatrix} \mathbf{I}_{n_n} & \mathbf{0} \\ \mathbf{0} & \mathbf{0} \end{bmatrix}. \tag{9}$$

With this choice, the term $d\mathbf{W}/d\beta$ in the right-hand side of Eq. 8 is identically a zero matrix, $d\mathbf{W}/d\beta = \mathbf{0}$. Additionally, the constant W_0 is set to 1 in Eq. 6, $W_0 = 1$, so that the aeroelastic eigenvector $\boldsymbol{\phi}^{(j)}$ is scaled as:

$$\boldsymbol{\phi}^{(j)} = \frac{\boldsymbol{\phi}_0^{(j)}}{\sqrt{\left(\boldsymbol{\phi}_0^{(j)}\right)^T \mathbf{W} \boldsymbol{\phi}_0^{(j)}}},$$

with $\boldsymbol{\phi}_0^{(j)} \in \mathbb{C}^{2n_h+n_a}$ the unscaled eigenvector obtained by direct solution of Eq. 2 and $\mathbf{W}$ given in Eq. 9.

As shown by Kaiser and Quero [21] the aeroelastic derivatives depend on the representation used for the aerodynamic term in the complex Laplace domain. In particular, due to the different approximations used by the *p-k* and *g* methods in representing the aerodynamic term, they provide different derivatives even at parameter combinations where the aeroelastic damping (real part of the aeroelastic eigenvalue) is zero, that is, at the flutter onset. In contrast, the aeroelastic derivatives provided by the solution of the (complex) linear Eq. 8 considers the true aeroelastic damping.

For the interested reader the explicit derivatives $d\mathbf{A}_{ae}/d\beta$ and $d\mathbf{E}_{ae}/d\beta$ required for the right-hand side term of Eq. 8 are provided in Appendix A for cases 1 through 3.

2.2 Mode tracking algorithm

In order to apply a mode tracking algorithm, after the determination of the aeroelastic eigensolution by solving Eq. 2, the first-order approximation of the eigensolution provided by Eq. 4 is used (with the derivatives provided by Eq. 8) together with a scalar which combines information from both the eigenvalue and eigenvector [28]:

$$\theta_k = \left| \mathrm{Im}\left\{\tilde{\lambda}^{(j+1)}\right\} - \mathrm{Im}\left\{\lambda_k\right\} \right| \left(1 - \sqrt{\mathrm{MAC}_k^{(j+1)}}\right), \quad k = 1, ..., 2n_h + n_a, \tag{10}$$

where the mean assurance criterion (MAC) takes values in the interval $[0, 1]$:

$$\mathrm{MAC}_k^{(j+1)} = \frac{\left| \left(\tilde{\boldsymbol{\phi}}^{(j+1)}\right)^* \boldsymbol{\phi}_k \right|^2}{\left(\left(\tilde{\boldsymbol{\phi}}^{(j+1)}\right)^* \tilde{\boldsymbol{\phi}}^{(j+1)}\right) \left(\boldsymbol{\phi}_k^* \boldsymbol{\phi}_k\right)},$$

and * represents the conjugate transpose of the aeroelastic eigenvector. The corresponding eigenvalue and eigenvector at the current stage is then determined by the index $\tilde{k}$ which produces the smallest value of the scalar $\theta_{\tilde{k}}$,

$$\tilde{k} = \underset{k \subset \{1,\ldots,2n_h+n_a\}}{\text{argmin}} \quad \theta_k,$$

so that $\lambda^{(j+1)} = \lambda_{\tilde{k}}$ and $\boldsymbol{\phi}^{(j+1)} = \boldsymbol{\phi}_{\tilde{k}}$.

In this work different scalars to that defined in Eq. 10 have been tested, showing a robust mode tracking for several scalar definitions which use the aeroelastic eigensolution information, pointing out the suitability of considering the aeroelastic derivatives in the mode tracking algorithm. For instance, the following scalar:

$$\theta_k = \frac{\left|\tilde{\lambda}^{(j+1)} - \lambda_k\right|}{< \tilde{\boldsymbol{\phi}}^{(j+1)}, \boldsymbol{\phi}_k >}, \quad k = 1, ..., 2n_h + n_a, \tag{11}$$

with the dedicated scalar product $< \tilde{\boldsymbol{\phi}}^{(j+1)}, \boldsymbol{\phi}_k >$ as defined by Van Zyl [16] delivers the same sorting of the eigensolutions for all cases investigated in Section 3.

Lastly, a predictor-corrector scheme [2, 19, 20] may readily be combined with the proposed mode tracking algorithm in order to adapt the parameter interval $\Delta\beta$ in case a difference between the expected eigensolution as predicted by Eq. 4, according to the scalar values defined in Eq. 10 or Eq. 11, is above an specified tolerance value θ_0, that is, $\theta_{\tilde{k}} > \theta_0$. However, the predictor-corrector scheme was not required for the applications of Section 3, with the chosen parameter intervals delivering a proper mode tracking of the aeroelastic eigensolutions.

3 APPLICATION CASES

In this section the *p-L* flutter solution method together with the mode tracking algorithm presented in Section 2 is applied to two different configurations. The first one corresponds to a well-known aeroelastic configuration consisting of a NACA64A010 airfoil in a range of Mach numbers and a two-dimensional structural model with 2 dof (heave and pitch) [29–31]. The second one is the CRM/FERMAT configuration representing a transport aircraft with the unsteady aerodynamics described by a potential compressible flow and a dedicated finite-element structural model for the stiffness matrix together with distributed masses [32, 33].

3.1 2 dof airfoil

In order to show the suitability of the *p-L* method for configurations requiring a high-fidelity description of the unsteady aerodynamics, the computational fluid dynamics (CFD) solver TAU [34], developed at the DLR, is chosen for the GAF computation. TAU assumes an unstructured finite-volume spatial discretization of the RANS equations, whereby the convective fluxes are discretized with a second-order central scheme. The steady solution is found by a local time stepping marching scheme in a first-order implicit backward-Euler form, which linear solution for each time step is iteratively obtained by application of a lower-upper symmetric Gauss-Seidel (LU-SGS) scheme [35]. The one equation model of Spalart and Allmaras [36], which has been extensively applied to aerospace applications, is chosen as turbulence closure

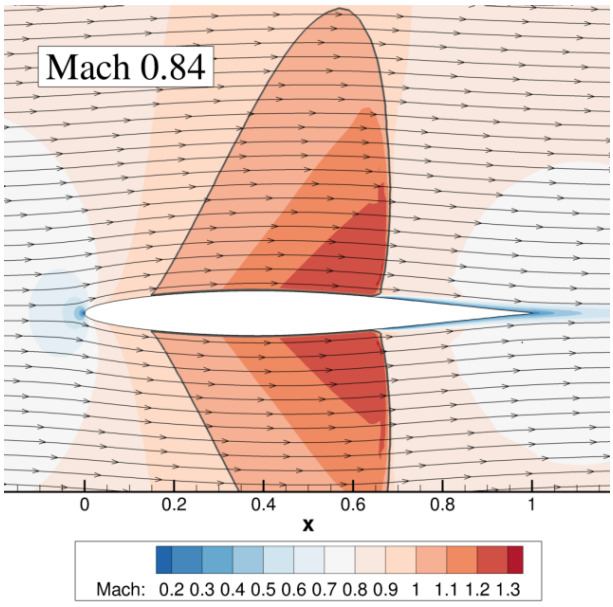

Figure 1: NACA64A010, Mach number 0.84 and angle of attack 0 (deg). Reynolds number 12.5 million and freestream temperature 288 (K).

model. For the GAF computation as function of the reduced frequency, from which the aerodynamic coefficients are obtained, a linear frequency domain (LFD) solver [37] is employed. This assumes a linear behavior of the unsteady RANS equations around a steady-state and solves for selected reduced frequency values. Note that by virtue of Lyapunov's indirect theorem [38], the linearized problem can be readily applied for the determination of the flutter boundary as a stability problem. As for the numerical LFD solver itself, a Krylov generalized minimal residual (GMRES) is used.

The computational mesh consists of around $24 \cdot 10^4$ cells, with more than 300 cells over each of the upper and lower surfaces of the airfoil. An O-grid surrounds the airfoil and contains 90 cells perpendicular to the airfoil contour, from which the first cell to the airfoil has a size of 10^{-6} times the airfoil chord, ensuring an y^+ value [39] below 1 for the boundary layer.

Several Mach numbers in the transonic region have been considered, ranging from 0.6 to 0.86 and an incremental value of 0.025, so as to numerically represent the transonic dip (drop in the flutter boundary limit) associated to the existence of recompression shocks. The angle of attack of the symmetric NACA64A010 has been fixed to zero, whereby the Reynolds number is $Re = 12.5$ million and the freestream temperature 288.15 (K). Fig. 1 shows the local Mach number distribution for the flow surrounding the airfoil at a freestream Mach number value of 0.84. There, the recompression shocks typical of the transonic regime are clearly visible.

The structural model is represented by 2 dof corresponding to the heave (h, positive downwards) and pitch (θ, positive nose-up) motions, where the airfoil rotates around the elastic axis. In this case the flutter equation is usually written in nondimensional form, which in the time domain reads [30]:

$$\begin{bmatrix} 1 & x_\theta \\ x_\theta & r_\theta^2 \end{bmatrix} \frac{d^2}{dt^2}\left(\begin{bmatrix} h/L_{ref} \\ \theta \end{bmatrix}\right) + \begin{bmatrix} g_s\omega_h & 0 \\ 0 & g_s r_\theta^2 \omega_\theta \end{bmatrix} \frac{d}{dt}\left(\begin{bmatrix} h/L_{ref} \\ \theta \end{bmatrix}\right) + \begin{bmatrix} \omega_h^2 & 0 \\ 0 & (r_\theta \omega_\theta)^2 \end{bmatrix} \begin{bmatrix} h/L_{ref} \\ \theta \end{bmatrix} = \frac{1}{\mu\pi}\left(\frac{U_\infty}{L_{ref}}\right)^2 \begin{bmatrix} -c_l\left(\alpha_0, M_\infty, Re\right) \\ 2c_m\left(\alpha_0, M_\infty, Re\right) \end{bmatrix}, \tag{12}$$

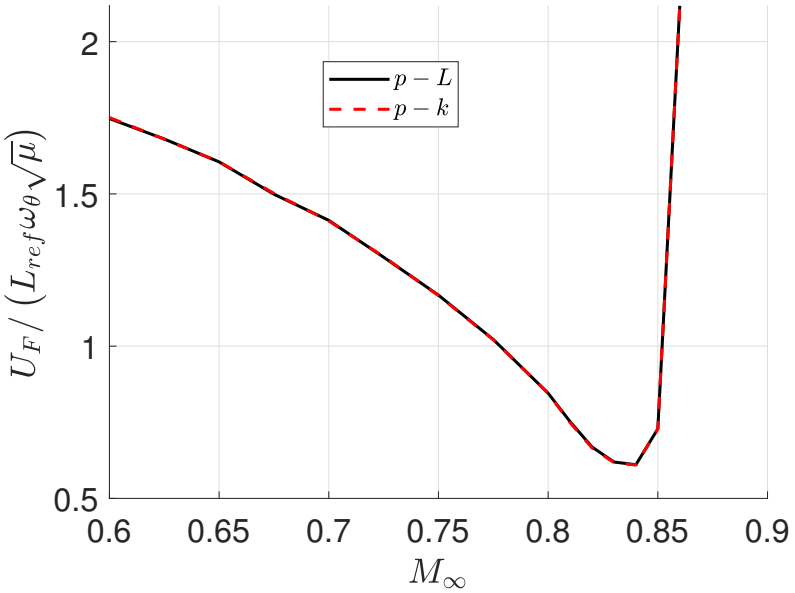

Figure 2: Flutter speed index $U_F/\left(\omega_\theta L_{ref}\sqrt{\mu}\right)$ against the Mach number M_∞ for the Isogai case A [29] as obtained by the *p-k* and *p-L* methods.

with $x_\theta = e - a$ the nondimensional static unbalance, r_θ the nondimensional moment of inertia, g_s the structural modal damping and the wind-off bending and torsional frequencies are represented by ω_h and ω_θ in (rad/s). The nondimensional position of the center of gravity is given by e, whereas the nondimensional (after dividing by the semichord $c/2$) location of the elastic axis is denoted by a, both relative to the midchord position. The reference length L_{ref} is equal to the semichord $c/2$ and μ denotes the mass ratio. The aerodynamic forces are represented by the lift and pitch moment (at the elastic axis location) coefficients c_l and c_m, depending on the steady angle of attack α_0 which has been set to zero, the Mach number M_∞ and the Reynolds number Re. Based on references [29–31], the following parameter values have been chosen:

$$L_{ref} = 0.5 \text{ (m)},\ a = -2,\ g_s = 0,\ x_\theta = 1.8,\ r_\theta^2 = 3.48,\ \mu = 60, \omega_h/\omega_\theta = 1.$$

In order to find the airspeed value U_F corresponding to the flutter onset, a sweep in the velocity U_∞ with an interval $\triangle\beta = \triangle U_\infty = 1$ (m/s) is done for each Mach number value, neglecting the dependency of the aerodynamic coefficients on the Reynolds number Re. Due to the nondimensional formulation in Eq. 12 the resulting flutter speed index $U_F/\left(\omega_\theta L_{ref}\sqrt{\mu}\right)$ depends on the ratio ω_h/ω_θ and not on the values ω_h and ω_θ independently [29, 31, 40]. Thus the frequency value ω_h may be chosen in order to achieve a resulting Reynolds number corresponding to U_F close to the one used in the LFD computations, minimizing the potential influence of Re in the aerodynamic coefficients. The value $\omega_h = 100$ (rad/s), as used by Edwards et al. [30], ensures this.

Fig. 2 shows a comparison between the nondimensional flutter speed $U_F/\left(\omega_\theta L_{ref}\sqrt{\mu}\right)$ as obtained by the classical *p-k* and the *p-L* method with the present mode tracking algorithm as described in Section 2.2, capturing the transonic dip region common to this regime. For this particular airfoil configuration, the original tracking criterion proposed in [5] is also able to properly track the aeroelastic eigensolution ultimately leading to the determination of the flutter onset.

3.2 CRM/FERMAT configuration

Next, a long-range transport aircraft configuration corresponding to the NASA common research model (CRM) geometry [32] and provided by Klimmek [33] is considered. The C2 case has been chosen, corresponding to a mass equal to the maximum takeoff weight of 260000 (kg). The structural damping has been set to zero. As for the aerodynamic model the modified double lattice method (DLM) valid throughout the complex plane [4] with a total of 2150 aerodynamic panels resulting has been used, see Fig. 3. Note that for *p-k*, *g* and *p-L* methods only the values at the imaginary axis are required. A more detailed description of the structural and aerodynamic models can be found in Klimmek [33].

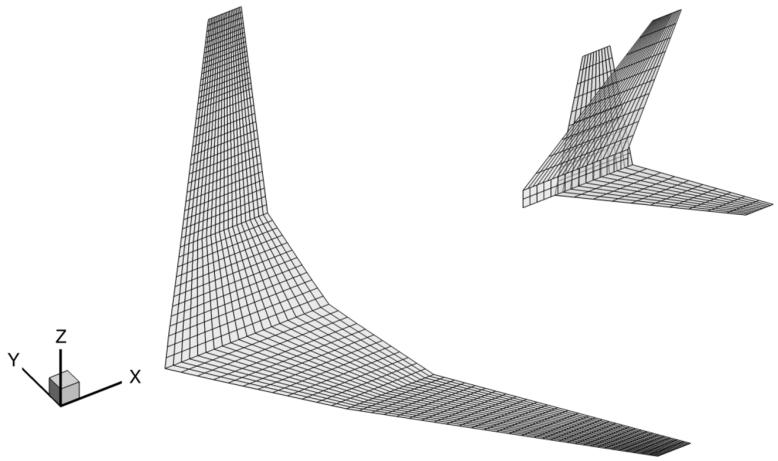

Figure 3: Aerodynamic boxes for the CRM/FERMAT configuration.

In order to obtain the evolution of the aeroelastic modes the Mach number M_∞ and the density value ρ_∞ are fixed to $M_\infty = 0.86$ and $\rho_\infty = 1.225$ (kg/m^3) respectively and a sweep in the airspeed value U_∞, $\triangle\beta = \triangle U_\infty$, corresponding to an increase in the dynamic pressure q_{dyn} of 1010 (Pa) is carried out. This corresponds to the case 1 described in Section 2.

Fig. 4 shows the evolution of the scaled damping $2g/k = 2\text{Re}\{\lambda\}/\text{Im}\{\lambda\}$ for a subset of the aeroelastic modes against the true airspeed U_∞ obtained after considering the first 44 flexible modes (for the mode numbering the mode 7 corresponds to the first flexible mode) with the *p-k* and *g* methods, GAAM [4] and the *p-L* method with the present mode tracking algorithm of Section 2.2. Additionally, the dynamic structural model has been *weakened* by scaling the generalized stiffness matrix by a factor of 1/2 while keeping the same eigenvectors in wind-off conditions and leaving the generalized mass equal to the identity matrix. It can be observed that only the *p-L* solution for increasing absolute values of g is indistinguishable from the reference GAAM. Note that for this configuration the original tracking algorithm proposed in [5], which does not make use of the aeroelastic derivatives, would not have been able to properly track the aeroelastic eigensolution.

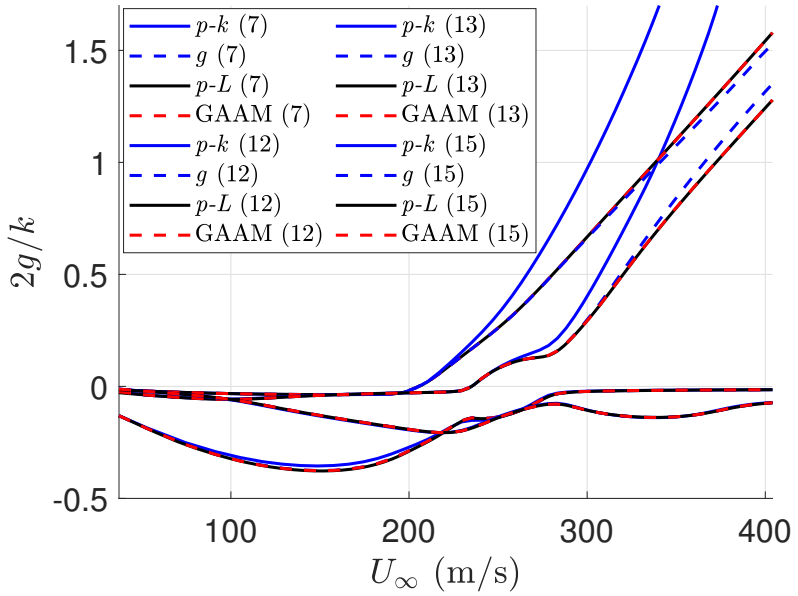

Figure 4: Damping ($2g/k$) at $M_\infty = 0.86$ and $\rho_\infty = 1.225$ (kg/m^3) against true airspeed U_∞ (m/s). Weakened CRM/FERMAT configuration.

To further highlight the potential difference between existing methods and the GAAM at lower speeds in the stable region, another modification of the CRM has been considered at a generalized level by multiplying the generalized mass and stiffness matrices by a factor of 1/2 and 3/2, respectively. For this modified dynamic structural properties the results are shown in Fig. 5, from which similar conclusions as for the previous case shown in Fig. 4 may be drawn, namely, that the *p-L* flutter solution method with the present mode tracking algorithm is able to truly represent the aerodynamic and thus aeroelastic damping as predicted by the reference provided by the GAAM.

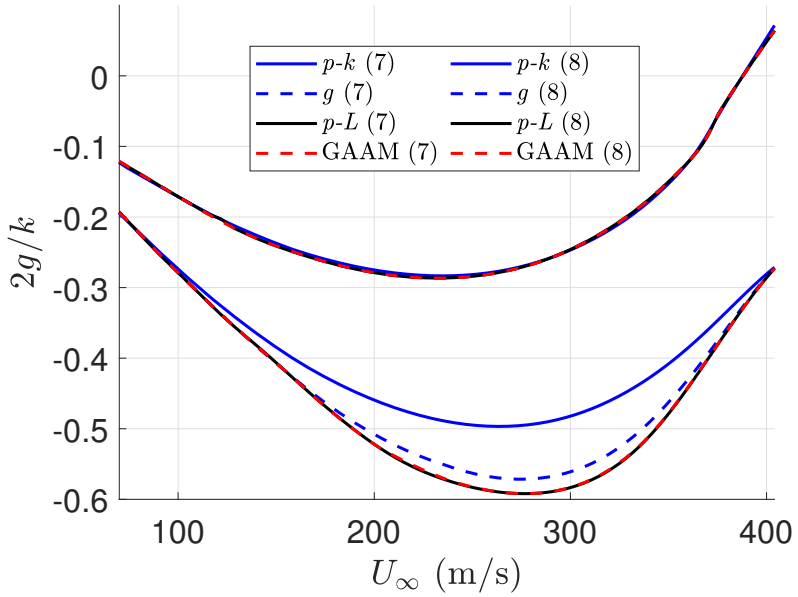

Figure 5: Damping ($2g/k$) at $M_\infty = 0.86$ and $\rho_\infty = 1.225$ (kg/m^3) against true airspeed U_∞ (m/s). Modified CRM/FERMAT configuration.

4 CONCLUSIONS

In this work the suitability of the *p-L* flutter solution method combined with an improved mode tracking algorithm for its application to the computation of aeroelastic modes of general configurations has been shown. To that aim, a refined mode tracking based on aeroelastic derivatives has been developed. The proposed method is shown to predict the flutter boundary limit of an airfoil with high-fidelity unsteady aerodynamics computed by a linearized CFD code. When applied to a general transport aircraft configuration and albeit using complex aerodynamic data solely over the imaginary axis, the predicted damping curves from the *p-L* method are in agreement with the reference GAAM, based on a modified DLM valid throughout the complex plane. This is true for the complete range of parameter values, unlike for the classical *p-k* and *g* flutter solution methods.

ACKNOWLEDGMENTS

This work has been funded within the frame of the Joint Technology Initiative JTI Clean Sky 2, AIRFRAME Integrated Technology Demonstrator platform AIRFRAME ITD (contract N. CSJU-CS2-GAM-AIR-2014-15-01 Annex 1, Issue B04, October 2nd, 2015) being part of the Horizon 2020 research and Innovation framework program of the European Commission.

APPENDIX A

In this section the analytical derivatives in Eq. 8 for different cases of the parameter β are provided. In all three cases considered the Mach number is constant, $M_\infty = M_0$, and thus $d\mathbf{E}_{ae}/d\beta = \mathbf{0}$.

Case 1: $\beta = U_\infty$**,** $M_\infty = M_0$ **and** $\rho_\infty = \rho_0$ **constant**

$$\frac{d\mathbf{A}_{ae}}{dU_\infty} = \begin{bmatrix} \mathbf{0} & \mathbf{0} & \mathbf{0} \\ \mathbf{0} & \mathbf{0} & \mathbf{M}_{hh}^{-1}\left(\frac{3\rho_0 U_\infty^2}{2L_{ref}}\right)\mathbf{C}_a\left(M_0\right) \\ \mathbf{0} & \mathbf{0} & \left(\frac{1}{L_{ref}}\right)\mathbf{A}_a\left(M_0\right) \end{bmatrix}$$

Case 2: $\beta = \rho_\infty$**,** $M_\infty = M_0$ **and** $U_\infty = U_0$ **constant**

$$\frac{d\mathbf{A}_{ae}}{d\rho_\infty} = \begin{bmatrix} \mathbf{0} & \mathbf{0} & \mathbf{0} \\ \mathbf{0} & \mathbf{0} & \mathbf{M}_{hh}^{-1}\left(\frac{U_0^3}{2L_{ref}}\right)\mathbf{C}_a\left(M_0\right) \\ \mathbf{0} & \mathbf{0} & \mathbf{0} \end{bmatrix}$$

Case 3: $\beta = h$**,** $M_\infty = M_0$ **constant and atmospheric relations**

$$\frac{d\mathbf{A}_{ae}}{dh} = \begin{bmatrix} \mathbf{0} & \mathbf{0} & \mathbf{0} \\ \mathbf{0} & \mathbf{0} & \mathbf{M}_{hh}^{-1}\left(\frac{M_0^3 a_\infty}{2L_{ref}}\right)\left[a_\infty^2\frac{d\rho_\infty}{dh} + \left(\frac{3\gamma R_g}{2}\right)\rho_\infty\frac{dT_\infty}{dh}\right]\mathbf{C}_a\left(M_0\right) \\ \mathbf{0} & \mathbf{0} & \left(\frac{M_0\gamma R_g}{2L_{ref}a_\infty}\right)\frac{dT_\infty}{dh}\mathbf{A}_a\left(M_0\right) \end{bmatrix}$$

The term dT_∞/dh can be readily computed by using the standard atmospheric relations and considering the appropriate atmospheric level [23].

5 REFERENCES

[1] Hassig, H. (1971). An approximate true damping solution of the flutter equation by determinant iteration. *Journal of Aircraft*, 8(11), 885–889. https://doi.org/10.2514/3.44311.

[2] Chen, P. (2000). Damping perturbation method for flutter solution: The g-method. *AIAA Journal*, 38(9), 1519–1524. https://doi.org/10.2514/2.1171.

[3] Edwards, J. and Wieseman, C. (2008). Flutter and divergence analysis using the generalized aeroelastic analysis method. *Journal of Aircraft*, 45(3), 906–915. https://doi.org/10.2514/1.30078.

[4] Quero, D. (2022). Modified doublet lattice method for its analytical continuation in the complex plane. *Journal of Aircraft*, 59(3). https://doi.org/10.2514/1.C036453.

[5] Quero, D., Vuillemin, P., and Poussot-Vassal, C. (2021). A generalized eigenvalue solution to the flutter stability problem with true damping: The *p-L* method. *Journal of Fluids and Structures*, 103(103266). https://doi.org/10.1016/j.jfluidstructs.2021.103266.

[6] Roger, K. L. (1977). Airplane math modeling methods for active control design. *AGARD-CP-228*, 4.1–4.11.

[7] Karpel, M. (1982). Design for active flutter suppression and gust alleviation using state-space aeroelastic modeling. *Journal of Aircraft*, 19(3), 221–227. https://doi.org/10.2514/3.57379.

[8] Morino, L., Mastroddi, F., Troia, R. D., et al. (1995). Matrix fraction approach for finite-state aerodynamic modeling. *AIAA Journal*, 33(4), 703–711. https://doi.org/10.2514/3.12381.

[9] Pasinetti, G. and Mantegazza, P. (1999). Single finite states modeling of aerodynamic forces related to structural motions and gusts. *AIAA Journal*, 37(5), 604–612. https://doi.org/10.2514/2.760.

[10] Ripepi, M. and Mantegazza, P. (2013). Improved matrix fraction approximation of aerodynamic transfer matrices. *AIAA Journal*, 51(5), 1156–1173. https://doi.org/10.2514/1.J052009.

[11] Crouch, J., Garbaruk, A., Magidov, D., et al. (2009). Origin of transonic buffet on aerofoils. *Journal of fluid mechanics*, 628, 357–369. https://doi.org/10.1017/S0022112009006673.

[12] Gao, C. and Zhang, W. (2020). Transonic aeroelasticity: A new perspective from the fluid mode. *Progress in Aerospace Sciences*, 113, 100596. https://doi.org/10.1016/j.paerosci.2019.100596.

[13] Nitzsche, J. (2009). A numerical study on aerodynamic resonance in transonic separated flow. In *IFASD Conference Proceedings*. https://elib.dlr.de/61964/1/J._Nitzsche_-_A_NUMERICAL_STUDY_ON_AERODYNAMIC_RESONANCE.pdf, accessed 13 May 2022.

[14] Van Zyl, L. (2001). Aeroelastic divergence and aerodynamic lag roots. *Journal of Aircraft*, 38(3), 586–588. https://doi.org/10.2514/2.2806.

[15] Colo, L., Broux, G., and Garrigues, E. (2019). A new flutter prediction algorithm to avoid p-k method shortcomings. In *IFASD Conference Proceedings*. https://www.asdjournal.org/public/Proceedings/IFASD_2019/IFASD-2019-072.pdf, accessed 13 May 2022.

[16] Van Zyl, L. (1993). Use of eigenvectors in the solution of the flutter equation. *Journal of Aircraft*, 30(4), 553–554. https://doi.org/10.2514/3.46380.

[17] Eldred, M., Venkayya, V., and Anderson, W. (1995). New mode tracking methods in aeroelastic analysis. *AIAA journal*, 33(7), 1292–1299. https://doi.org/10.2514/3.12552.

[18] Hang, X., Fei, Q., and Su, W. (2019). On tracking aeroelastic modes in stability analysis using left and right eigenvectors. *AIAA Journal*, 57(10), 4447–4457. https://doi.org/10.2514/1.J057297.

[19] Cardani, C. and Mantegazza, P. (1978). Continuation and direct solution of the flutter equation. *Computers and Structures*, 8(2), 185 – 192. https://doi.org/10.1016/0045-7949(78)90021-4.

[20] Meyer, E. (1988). Application of a new continuation method to flutter equations. In *29th AIAA Structures, Structural Dynamics and Materials Conference*. Williamsburg, VA, USA. https://doi.org/10.2514/6.1988-2350.

[21] Kaiser, C. and Quero, D. (2022). Effect of aerodynamic damping approximations on aeroelastic eigensensitivities. *Aerospace*, 9(3). https://doi.org/10.3390/aerospace9030127.

[22] Moler, C. and Stewart, G. (1973). An algorithm for generalized matrix eigenvalue problems. *SIAM Journal on Numerical Analysis*, 10(2), 241–256. https://doi.org/10.1137/0710024.

[23] Atmosphere, U. S. (1976). Technical report NASA-TM-X-74335. *National Aeronautics and Space Administration*.

[24] Vojkovic, T., Vuillemin, P., Quero, D., et al. (2022). Parametric reduced-order modeling of aeroelastic systems. *International Conference on Mathematical Modelling (MATHMOD)*.

[25] Zhu, J., Wang, Y., Pant, K., et al. (2017). Genetic algorithm-based model order reduction of aeroservoelastic systems with consistent states. *Journal of aircraft*, 54(4), 1443–1453. https://doi.org/10.2514/1.C034129.

[26] Krolick, W., Shu, J., Wang, Y., et al. (2021). State consistence of data-driven reduced order models for parametric aeroelastic analysis. *SN Applied Sciences*, 3(2), 1–24. https://doi.org/10.1007/s42452-021-04252-w.

[27] Iannelli, A., Fasel, U., and Smith, R. (2021). The balanced mode decomposition algorithm for data-driven lpv low-order models of aeroservoelastic systems. *Aerospace Science and Technology*, 115, 106821. https://doi.org/10.1016/j.ast.2021.106821.

[28] Yue, C. and Zhao, Y. (2021). Interpolation-based modeling methodology for efficient aeroelastic control of a folding wing. *International Journal of Aerospace Engineering*, 2021. https://doi.org/10.1155/2021/8609211.

[29] Isogai, K. (1980). Numerical study of transonic flutter of a two dimensional airfoil. *NAL TR-716*.

[30] Edwards, J., Bennett, R., Whitlow Jr, W., et al. (1983). Time-marching transonic flutter solutions including angle-of-attack effects. *Journal of Aircraft*, 20(11), 899–906. https://doi.org/10.2514/3.48190.

[31] Schulze, S. (1998). Transonic aeroelastic simulation of a flexible wing section. *AGARD Report R-822: Numerical Unsteady Aerodynamic and Aeroelastic Simulation*, 10–1.

[32] Vassberg, J., Dehaan, M., Rivers, M., et al. (2008). Development of a common research model for applied cfd validation studies. In *26th AIAA applied aerodynamics conference*. Honolulu, Hawaii, USA. https://doi.org/10.2514/6.2008-6919.

[33] Klimmek, T. (2014). Parametric set-up of a structural model for fermat configuration aeroelastic and loads analysis. *Journal of Aeroelasticity and Structural Dynamics*, 3(2). https://doi.org/10.3293/asdj.2014.27.

[34] Schwamborn, D., Gerhold, T., and Heinrich, R. (2006). The DLR TAU-code: recent applications in research and industry. In *ECCOMAS CFD conference*.

[35] Yoon, S. and Jameson, A. (1988). Lower-upper symmetric-Gauss-Seidel method for the Euler and Navier-Stokes equations. *AIAA journal*, 26(9), 1025–1026. https://doi.org/10.2514/3.10007.

[36] Spalart, P. and Allmaras, S. (1992). A one-equation turbulence model for aerodynamic flows. In *30th AIAA Aerospace Sciences Meeting and Exhibit*. https://doi.org/10.2514/6.1992-439.

[37] Thormann, R. and Widhalm, M. (2013). Linear-frequency-domain predictions of dynamic-response data for viscous transonic flows. *AIAA journal*, 51(11), 2540–2557. https://doi.org/10.2514/1.J051896.

[38] Khalil, H. and Grizzle, J. (2002). *Nonlinear systems*. Prentice hall Upper Saddle River, New Jersey.

[39] Schlichting, H. and Gersten, K. (2003). *Boundary-layer theory*. Springer Science & Business Media. https://doi.org/10.1007/978-3-642-85829-1.

[40] Theodorsen, T. and Garrick, I. (1940). Mechanism of flutter: a theoretical and experimental investigation of the flutter problem. *NACA Technical Report 685*.

COPYRIGHT STATEMENT